NASA TECHNICAL MEMORANDUM

NASA TM X-1597

NASA TM X-1597

TARGET PRESSURE AND DAMAGE DATA FROM IMPACTS BY EXPLOSIVELY PROPELLED PROJECTILES

by A. B. Wenzel and Nestor Clough

Lewis Research Center

Cleveland, Ohio

NATIONAL AERONAUTICS AND SPACE ADMINISTRATION • WASHINGTON, D. C. • JUNE 1968

NASA TM X-1597

TARGET PRESSURE AND DAMAGE DATA FROM IMPACTS BY EXPLOSIVELY PROPELLED PROJECTILES

By A. B. Wenzel and Nestor Clough

Lewis Research Center
Cleveland, Ohio

NATIONAL AERONAUTICS AND SPACE ADMINISTRATION

For sale by the Clearinghouse for Federal Scientific and Technical Information
Springfield, Virginia 22151 – CFSTI price $3.00

ABSTRACT

Data on maximum shock-generated pressures at several axial positions in 1100-0 aluminum and on crater dimensions in 316-stainless steel were obtained from impacts by explosively-fired aluminum projectiles at the facilities of the General Motors Defense Research Laboratories, Santa Barbara, California. The aluminum projectiles with mass ranging from 0.408 to 0.626 grams, impacted the targets at velocities of 11 km/sec. Comparisons of pressure data with similar data from light-gas gun impacts are included, together with a discussion of the "throw-off pellet" technique used to obtain axial pressures.

STAR Category 32

TARGET PRESSURE AND DAMAGE DATA FROM IMPACTS BY EXPLOSIVELY PROPELLED PROJECTILES

by A. B. Wenzel* and Nestor Clough

Lewis Research Center

SUMMARY

This report presents the results of an experimental program conducted at General Motors Defense Research Laboratories under contract with the NASA-Lewis Research Center. The program had two objectives: (a) firing five (5) shots to obtain data on the axial variation of maximum shock-generated pressures in aluminum (1100-0) targets of varying thickness when impacted by an aluminum projectile at 11 kilometers per second; and (b) firing four (4) shots to obtain crater dimensions from aluminum impacts on (316) stainless steel at 11 kilometers per second.

The results of these nine shots were compared to similar light gas gun data obtained at lower velocities (5 to 9 km/sec). In general, the peak axial pressures measured from the explosive shots agreed very well with the light-gas-gun data obtained at lower velocities, whereas crater depths were somewhat less than the values obtained from comparable light-gas-gun data.

INTRODUCTION

One of the engineering problems confronting the space designer interested in determining design criteria for protecting space structures from meteoroid impact is the simulation of such an impact. Light-gas guns developed for such experimentation, have to date produced projectile velocities approaching the lower threshold of what is considered to be the meteoroid velocity spectrum. Explosive techniques produce projectile velocities greater than those attained by light-gas guns, but with certain disadvantages. The light-gas gun accelerates projectiles of known size, weight, and density; whereas these characteristics of explosively-accelerated projectiles must be deduced from data collected after the projectile is produced and is in flight to the target. It is therefore

*Allison Division of General Motors.

desirable to evaluate explosively-obtained data not only on its own but also in comparison to data theoretically and experimentally derived from the light-gas gun and other research sources.

The experiments described herein were conducted to determine the peak compression or shock wave pressure as a function of distance into the target. These data are useful in predicting thin target damage such as spall initiation, as well as being useful in Hugoniot determination. The program also provided some data on cratering into thick (10 cm) stainless steel blocks. These data are for comparison with light-gas-gun results obtained for similar materials at lower velocities.

DESCRIPTION OF TESTS

Test Equipment

The shaped-charge experiments were conducted at the Terminal Ballistics Laboratory of the General Motors Defense Research Laboratory. The laboratory's explosive facility consists of a building, 15 meters long and 4 meters high at the center point, designed to meet the safety requirements of a firing enclosure for explosive weights up to three pounds.

The device used to accelerate single projectiles up to 11 kilometer per second was an inhibited shaped-charge accelerator. This device employs basic shaped-charges techniques modified to produce a single pellet-like projectile rather than a long jet-like projectile (ref. 1). In brief, a cylindrical block of explosive about 7.6 centimeters long and 5.1 centimeters in diameter with a detonator attached to one end, forms the charge or explosive body of the device. A hollow cone of aluminum is inserted, point first, into the end opposite the detonator. When the charge is detonated, the detonation wave passes through the cone, the thin aluminum walls collapse and squirt forward. This process normally produces a long, rod-like projectile or jet; but in these tests, the inhibited shaped-charge design used produces a pellet of relatively short length-to-diameter ratio. In this design, an additional small amount of explosive attached to the side of the charge generates side pressures that destroy the tail of the emerging jet, leaving only a pellet to strike the target. The length-to-diameter (L/d) ratio of the pellet can be controlled from about 2 to 20, by varying the height of the inhibitor.

The projectile flight range is designed so that impact tests can be conducted at reduced pressures, if desired, and instrumented so that multiple orthogonal pictures can be made with flash radiography. Figure 1 shows three views of the range. The X-ray tube holders, impact chamber, blast deflector, and explosive charge holder are clearly labeled in the figure. The flight path of the projectile is approximately 1/2 meter from the explosive charge to the target.

Because of its short pulse duration and its ability to penetrate explosive products, flash radiography is an excellent technique for recording projectile characteristics and target behavior. The flash radiographic equipment was located in the impact chamber where the projectile in flight and the target behavior after impact could both be observed. The X-ray system consisted of five individual channels, each with a trigger amplifier. The system, in addition, includes the following three units: (1) a delay network for synchronizing the passing of the projectile in flight with the flash of the X-ray tube; (2) a 100-kilowatt storage bank with an appropriate network for providing 0.03-microsecond discharge times; and (3) five X-ray tubes fed by matched impedance coaxial cables. The storage banks are housed in the X-ray building, and the X-ray tubes are protected by steel pipes along the projectile flight line.

All tests are initiated from a panel housed in the fire-control trailer. The panel consists of a remote firing panel, six channels of counter chronographs to establish the time of the events, a console for the flash X-ray system, and several oscilloscopes for monitoring events in the range and calibrating the electronics equipment.

Radiographic Techniques

Flash radiographic equipment is located so that the projectile's position can be recorded orthogonally on the flight line at two stations: station one is near the shaped charge; station two around 1/2 meter away is near the target. Radiographic conditions are held constant during the firing of each lot of charges. A minimum of two stationary reference projectiles of known mass and dimensions, plus a step-wedge, are mounted in the chamber to be radiographed with the moving projectile. The step-wedge is made of step increases in thickness of the same material as the projectile, so that X-ray comparison of the projectile with an object of known opacity can be made. The location of the flight line is determined after each shot by the location of the crater in the target.

To establish parameters for the radiographic equipment, a static board, 20 centimeters by 26 centimeters with a 2 centimeter grid, is placed on the flight line. The board holds a number of reference projectiles of different shapes, masses, and densities. The distance from the X-ray source to the film, the distance from the projectile to the film, the discharge voltage, the shielding conditions, and the type of film used all contribute to the interpretation of the results. The magnification which occurs (parallax) when an object is not in direct contact with the film can be determined by measuring radiographs of the static board and comparing these with true dimensions. Once the magnification factor is known, measurements obtained directly from the film can be converted to actual projectile dimensions.

Projectile dimensions were obtained by measuring directly from the negative of

the X-ray film, since an error analysis indicated that this procedure was more accurate than other applicable methods.

Determination of Projectile Characteristics

Just before impact, measurements were made of the projectile velocity, length, diameter, and mass; after impact measurements were made of crater depth, diameter, volume, and target hardness below the crater.

Velocity. - Projectile velocity was determined by using the flash radiographic equipment located along the projectile flight line (fig. 1) and counter chronographs. The time between X-rays and the measured distance between projectile location along the flight line allowed the determination of projectile velocity just before impact within ±1 percent (ref. 2).

Length and diameter. - Projectile length and diameter were measured from orthogonal radiographs taken just before impact according to the procedure mentioned previously. The length and diameter were measured three times on the radiograph and the average of the three measurements were used in calculating the mass. The accuracy of the measured length and diameters is ±0.0406 centimeter (ref. 2).

Density. - Projectile density was determined by radiographic comparison of the test projectile and the two reference projectiles and the step-wedge. This measurement is regarded as a more accurate determination than the projectile dimensions.

Mass. - Projectile mass was calculated from the parallax-corrected projectile dimensions and the appropriate projectile density. Since, however, the projectiles are generally conical in shape, their outer boundaries are transparent to X-rays, so that mass calculated using the radiograph tends to be somewhat less than the true mass. Since the physical projectile measurements introduce the greatest source of error in the projectile mass determination, the projectile mass was also determined, for thick target shots, by using the equation (ref. 3),

$$V_c = 0.1(\rho_j)^{1/6}\left(\frac{1}{\rho_t}\right)^{1/2}\left(\frac{E}{B_{max}}\right) \tag{1}$$

where E is projectile kinetic energy ($1/2\ mV^2$) in joules, B_{max} is the maximum target Brinell Hardness Number, and V_c is crater volume in cubic centimeters (a list of symbols is given in the appendix). Equation (1) is an empirical relation determined for rods and jets of $L/d \geq 2$ (fig. 2). By using equation (1), it is therefore possible to calculate projectile mass without knowing L and d. The mass predicted by equation (1) is

stated to vary up to ±20 percent from the measured mass for light-gas gun projectiles.

When radiographs of the projectile and the actual crater dimensions were both available, the average of the two measurements was used as the reported mass of the projectile. (The agreement of the two masses was within the expected ±20 percent.) When crater dimensions were not available (as is the case when firing against thin targets), the mass was determined solely from the radiographs.

Crater measurements. - Crater volume was measured by filling the crater full of water from a burette. Crater depth, diameter, and hardness were obtained from measurements made on the target after it was sectioned.

Axial Pressure Measurements

The "throw-off pellet" technique was used to determine the average particle velocity associated with a shock wave at a free surface of the target (ref. 4). The technique involves the use of two sets of orthogonal X-ray channels to determine the velocity of a very thin pellet thrown off the free rear surface of the target directly after impact (fig. 3). The first set of orthogonal X-rays are triggered by a quartz pressure transducer placed on the rear surface of the target to sense the arrival of the shock front. The second set of X-rays are triggered by a time delay so that the pellet in flight is photographed twice on the same X-ray plate. Pellet velocity measurements are made within the first 10 centimeters of travel to minimize the effects of air drag.

The velocity of the pellet is essentially equal to the maximum velocity of the free surface of the target upon arrival of the shock wave, and this velocity is twice the average particle velocity of the shock wave portion captured by the pellet during the time of interaction (ref. 5). Thus the known particle velocity makes it possible to calculate the maximum shock pressure from the relation (ref. 5),

$$\sigma_M = \rho_t U \mu \tag{2}$$

where σ_M is the maximum shock pressure, ρ_t is the target density, U is the shock velocity, and μ is the particle velocity behind the shock. The shock velocity U is obtained from the Hugoniot of the material (ref. 5). Then, since the pellet velocity is twice the particle velocity behind the shock

$$\sigma_M = \rho_t \frac{UV_p}{2} \tag{3}$$

where V_p is the measured pellet velocity.

EXPERIMENTAL RESULTS

Pressure Measurements

Five shots were fired to obtain crater dimensions and axial pressures from impacts of aluminum projectiles of approximately 0.6 gram into 10 centimeters by 10 centimeters targets of varying thickness of 1100-0 aluminum. Shaped charges launched the projectiles at velocities in the region of 11 kilometers per second. An X-ray of a typical shaped charged projectile (shot number 496) is shown in figure 4.

The first shot (shot number 495) was a calibration shot to evaluate projectile characteristics and target behavior and to check the timing of the X-ray equipment. The remaining four shots (shots numbers 496, 501, 502, and 503) were fired to obtain axial pressure data. For these tests, the target blocks were varied in thickness. Because of the limited number of shots, the thicknesses of the targets (9.2, 7.3, 1.4, and 0.95 cm) were chosen to give data at relatively extreme points. The target impacted by shot number 496 was cut to two thicknesses to give two data points for one shot as shown in figure 5.

A summary of the test data is presented in table I. Velocity $V_{p,1}$, $V_{p,2}$, and $V_{p,3}$ in table I represent the pellet velocity measured by X-ray channels 1, 2, and 3; channel 3 being orthogonal to channels 1 and 2. Pressure σ_1, σ_2, and σ_3 represent the respective calculated pressures from the measured pellet velocities, according to equation (3). The "throw-off pellet" technique as described was used for shots numbers 495, 496, and 501. For shots numbers 502 and 503 due to the reduced target thickness, the free surface velocity is measured from the leading element of the bubble of debris generated (fig. 6). With this velocity and the Hugoniot of the material the maximum shock pressure was calculated from equation (3).

Figure 7 shows the results of these tests where maximum shock pressure against distance from point of impact is plotted. As seen from the faired curve, pressures for these impacts of approximately equal projectile mass and velocity are reasonably represented by an inverse power function of distance into the target. The data were based on the assumption that the free surface velocity is twice the particle velocity behind the shock in the material as described earlier.

Maximum shock-generated pressures are available from a formula derived in reference 4 from light-gas-gun data (spherical projectiles) and theoretical considerations. The formula is an engineering relation giving maximum shock wave pressures in aluminum (1100-0) as a function of distance into the target and of the radius of the projectile. From a straight line fitted through the calculated and experimental results as shown in figure 8 (from ref. 4), the following expression was obtained.

$$\sigma_M = \frac{1.234\,\sigma_H}{(R/R_o)^{1.6}}, \qquad R > 1.14\,R_o \tag{4}$$

Where σ_H is the Hugoniot pressure corresponding to the impact velocity, R is the distance from impact (target thickness), and R_o is the equivalent effective radius of the projectile. A comparison between the values predicted from equation (4) and the experimetally measured pressures is shown on figure 9. There is seen to be reasonable agreement between the predicted and experimentally measured pressures, even though the formula came mostly from spherical projectile data at velocities lower than the explosive tests.

Crater Coefficient

Four shots were fired using the shaped charge against 10 centimeters thick 316-stainless steel targets. These tests were made to provide crater data (volume, depth, and diameter) produced by an aluminum projectile of low L/d impacting at 11 kilometers per second. The results are given in table II. Before these data can be compared with light-gas gun data for spherical projectiles, the projectile shape factor must be determined. The projectile shape factor for projectiles of equal mass is defined in reference 2.

$$f_p = \frac{P_j}{P_s} = \frac{\text{penetration of cylinder of fixed L/d}}{\text{penetration of a sphere}}$$

where, in general f_p varies with the magnitude of L/d.

The shape factor, f_p, has been reported for aluminum, steel, and beryllium projectiles against aluminum targets in reference 2. For the aluminum targets for values of $L/d < 3$, f_p lies in the range of 1.1 to 1.5 for impacts at velocities around 7.5 kilometers per second. The values of f_p for the aluminum-steel combination tested herein have not as yet been determined. Since the value of f_p tends toward 1.0 as the impact velocity increases (ref. 2), an assumed value of $f_p = 1.0$ was used when comparing the explosive shot data to light-gas gun results obtained with spherical projectiles.

The following equation for predicting crater depth by impacting spherical projectiles has been extensively used (ref. 6):

$$\frac{P_s}{d_s} = \gamma\left(\frac{\rho_s}{\rho_t}\right)^{\varphi}\left(\frac{V}{\sqrt{\frac{E_t}{\rho_t}}}\right)^{2/3} \tag{5}$$

where P_s is the penetration depth, d_s is the projectile diameter, ρ_s the projectile

density, ρ_t the target density, φ a constant (1/2 or 2/3), V the impact velocity, E_t Young's modulus of the target, and γ is an empirical correlating factor (cratering coefficient).

A value of γ for spherical Pyrex projectiles impacting 316 stainless steel at room temperature has been reported in reference 7. For $\varphi = 1/2$, $\gamma = 1.68$ was obtained. More recent unpublished data with aluminum spheres impacting 316 stainless steel plates have become available, and these data will be used for the comparison.

Since for the jet projector shots, the projectile diameter in equation (5), is a rather elusive value compared to the volume, spherical projectile volume was substituted for diameter in equation (5) to yield

$$P_s = \gamma\left(\frac{6m}{\pi\rho_p}\right)^{1/3}\left(\frac{\rho_j}{\rho_t}\right)^{\varphi}\left(\frac{V}{\sqrt{\frac{E_t g}{\rho_t}}}\right)^{2/3} \tag{6}$$

where m is the projectile mass. Now for the jet shots, $P_j = f_p P_s$ so that

$$P_j = f_p\gamma\left(\frac{6m}{\pi\rho_j}\right)^{1/3}\left(\frac{\rho_j}{\rho_t}\right)^{\varphi}\left(\frac{V}{\sqrt{\frac{E_t g}{\rho_t}}}\right)^{2/3} \tag{7}$$

Solving for γ yields:

$$\gamma = \frac{P_j}{f_p\left(\frac{6m}{\pi\rho_j}\right)^{1/3}\left(\frac{\rho_j}{\rho_t}\right)^{\varphi}\left(\frac{V}{\sqrt{\frac{E_t g}{\rho_t}}}\right)^{2/3}} \tag{8}$$

Substitution of the respective values of projectile properties (table II) and assumed shape factor then yielded values of γ for the test shots.

Table III summarizes the results of these calculations as well as the results of two impacts by spherical aluminum projectiles launched by a light-gas gun. The table lists the calculated values of γ for φ equal to 1/2 and 2/3 and the various values used in equation (8) to calculate γ. For stainless steel, $E_t = 30\times10^6$ psi and $\rho_t = 8$ grams per

cubic centimeter. For aluminum, $\rho_p = 2.7$ grams per cubic centimeter. The table also lists the ratio of crater diameter to crater depth D/P for both the jet projector shots and the light-gas-gun shots. This parameter gives an indication of the inferred similarity of the impacts.

The values of D/P for the jet-projector shots and the light-gas-gun shots are seen to be very close, indicating similar crater shapes. The average values determined for γ for the jet projector shots were about 17 percent lower than the average values of γ obtained from light-gas-gun shots. These differences between jet-projector and light-gas-gun values of γ are not very great considering the unknowns implicit in the determination of the jet-projector values of γ.

As mentioned previously, the determinations of the projectile mass is not very precise and may vary by as much as ±20 percent. With γ proportional to mass to the 1/3 power, much of the 17 percent difference in the value of γ could thus be explained. Secondly, the value of $f_p = 1.0$ used for the jet-projector shots in equation (8) is for very high velocity cylinders impacting with their axis normal to the target. If the projectile impacts off-axis or in a skewed position, reference 2 indicates f_p can become less than 1.0. (In fig. 4, the projectile is seen to be skewed about 10^o to the flight path.) A reduced value of f_p will result in a larger value of γ (eq. (8)).

The differences in velocity regime of impact (light-gas gun 7.5 km/sec; explosive shots, 11.0 km/sec), as well as differences in the target material (the targets were not from the same heats nor did they have the same history of processing), may also be contributing factors to the observed differences in γ.

CONCLUDING REMARKS

The tests described herein showed the variation of shock pressure with target thickness for 1100-0 aluminum to be in relatively good agreement with similar data obtained by a different method. Small differences in the impact cratering coefficient were found when comparable data from light-gas gun impacts were compared to the data reported herein. However, it is felt that the differences are within the experimental unknowns. Although these results were obtained from a relatively few impacts, the general agreement nevertheless gives support to the proposal for using the explosive method of projectile formation for extending the velocity range of impact-phenomena research.

Lewis Research Center,
National Aeronautics and Space Administration,
Cleveland, Ohio, February 28, 1968,
120-27-04-36-22.

APPENDIX - SYMBOLS

B_{max}	Maximum target hardness, Brinell Hardness Number
D	crater diameter
d	projectile diameter
E	projectile kinetic energy
E_t	modulus of elasticity
f_p	projectile shape factor
g	gravitational constant
L	projectile length
m	projectile mass
P	crater depth
R	target thickness
R_o	projectile equivalent radius
U	shock velocity
V	projectile velocity
V_c	crater volume
V_p	pellet velocity
γ	cratering coefficient
μ	particle material velocity behind shock in target
ρ	projectile density
ρ_t	target density
σ_H	Hugoniot pressure
σ_M	maximum shock pressure
φ	constant

Subscripts:

j	jet-projector projectile
s	spherical projectile (light-gas gun)
1, 2, 3	successive values from X-ray channels

REFERENCES

1. Wenzel, A. B.; and Gehring, J. W.: Techniques for Launching 0.01- to 25-gram Discrete Projectiles at Velocities up to 54,100 ft/sec. Proceedings of the Fourth Hypervelocity Techniques Symposium. University of Denver, 1966, pp. 379-407.

2. Wenzel, A. B.; and Gehring, J. W.: Hypervelocity Impact Studies Against Apollo-Type Structures up to 16.5 km/sec. Rep. No. TR 65-56, General Motors Corp., Aug. 1965.

3. Christman, D. R.; and Gehring, J. W.: Penetrative Mechanisms of High Velocity Projectiles. Rep. No. TR 65-50, General Motors Corp., July 1965.

4. Meyers, C. L.; and Charest, J. A.: Research on the Properties of Optimum Meteoroid Shields. Rep. No. TR 64-48 (NASA CR-64934), General Motors Corp., Sept. 1964.

5. Charest, Jacques A.: Measurements of Shock Wave Pressures Generated by Hypervelocity Impacts in Aluminum. Rep. No. TR 64-58 (NASA CR-78399), General Motors Corp., Nov. 1964.

6. Loeffler, I. J.; Lieblein, Seymour; and Clough, Nestor: Meteoroid Protection for Space Radiators. Power Systems for Space Flight. Vol. 11 of Progress in Astronautics and Aeronautics. Morris Zipkin and Russell N. Edwards, eds., Academic Press, 1963, pp. 551-579.

7. Clough, Nestor; Diedrich, James H.; and Lieblein, Seymour: Results of Hypervelocity Impacts into Space Radiator Materials. Presented at the AIAA First Rankine Cycle Space Power Systems Specialists Conference, Cleveland, Oct. 26-28, 1965.

TABLE I. - AXIAL PRESSURE MEASUREMENTS FROM ALUMINUM SHAPED-CHARGE PROJECTILES IMPACTING ALUMINUM (1100-0) TARGETS

Shot	Projectile			Target thickness, R, cm	Pellet velocity, km/sec			Pressure, kbars			Average pressure, σ, kbars
	Velocity, V, km/sec	Shape, L/d	Mass, m, g		$V_{p,1}$	$V_{p,2}$	$V_{p,3}$	σ_1	σ_2	σ_3	
495	10.93	5.6	0.839	8.9	0.224	0.216	0.210	17	16.9	16.8	16.9
496	11.0	3.2	.608	9.2	.090	.118	.108	7	9	8.5	8.4
	11.0	3.2	.608	7.3	.128	.158	.148	10	12.8	12	11.6
[a]501	-----	---	-----	----	-----	-----	-----	--	-----	-----	-----
502	11.5	5	.626	.95	(b)	(b)	(b)	(b)	(b)	(b)	(b)
503	11.35	3.4	.562	1.4	-----	1.52	1.76	--	310	282	296

[a]Bad shot.

[b]X-ray did not trigger.

TABLE II. - IMPACT MEASUREMENTS OF ALUMINUM SHAPED-CHARGE PROJECTILE IMPACTING STAINLESS-STEEL (316) TARGETS

Shot	Projectile			Target thickness, R, cm	Crater depth, P_j, cm	Crater diameter, D_j, cm	Crater volume, V_c, cm^3	Target hardness, Brinell Hardness Number
	Velocity, V, km/sec	Shape, L/d	Mass, m, g					
497	11.05	2.8	0.567	10.1	1.1	2.67	2.42	128
498	11.36	1.6	.460	10.1	.927	2.29	2.30	128
499	11.30	(a)	.474	10.1	.818	1.98	1.29	122
[b]500	-----	---	-----	----	-----	----	----	---

[a]Irregular.

[b]Bad shot, projectile hit deflector.

TABLE III. - COMPARISON OF CRATERING RESULTS

Mass	Crater diameter to depth ratio, (D/P)	Calculated cratering coefficient, γ, at-	
		$\varphi = 1/2$	$\varphi = 2/3$
Jet projector; velocity, V = 11 km/sec			
0.567	2.43	1.52	1.84
.460	2.47	1.36	1.63
.474	2.42	1.19	1.43
		1.36 av	1.63 av
Light-gas gun; velocity, V = 7.5 km/sec			
0.0468	2.50	1.63	1.95
.0468	2.32	1.65	1.98
		1.64 av	1.96 av

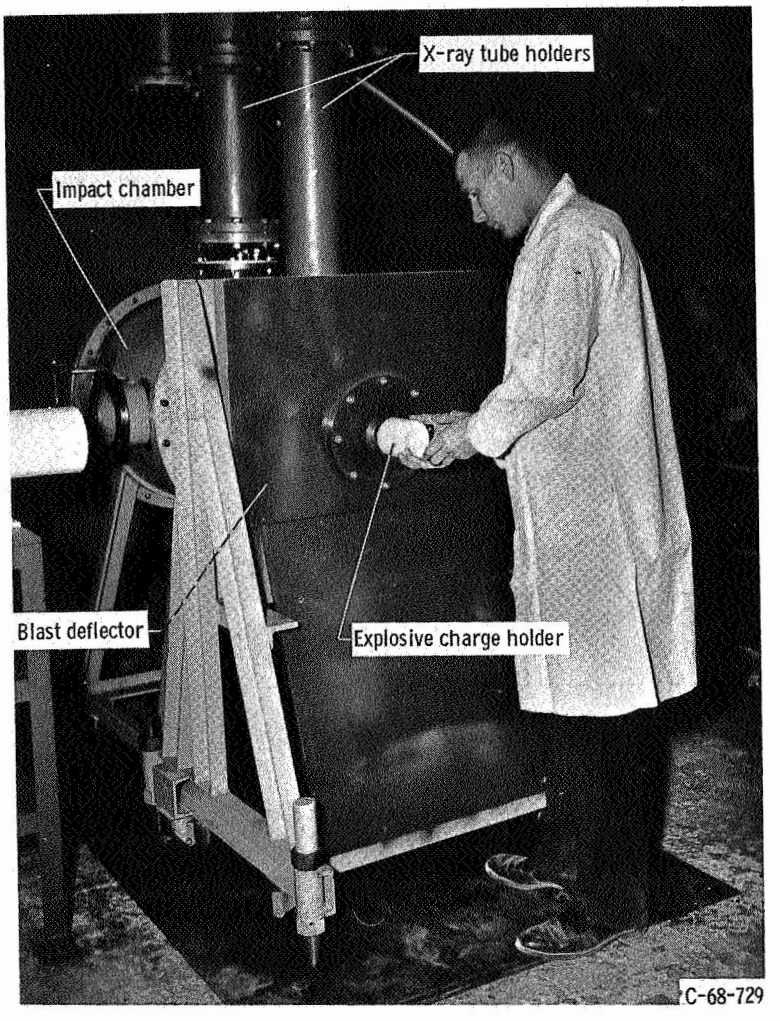

(a) Front view.

Figure 1. - Terminal Ballestics Laboratory Explosives Range Facility.

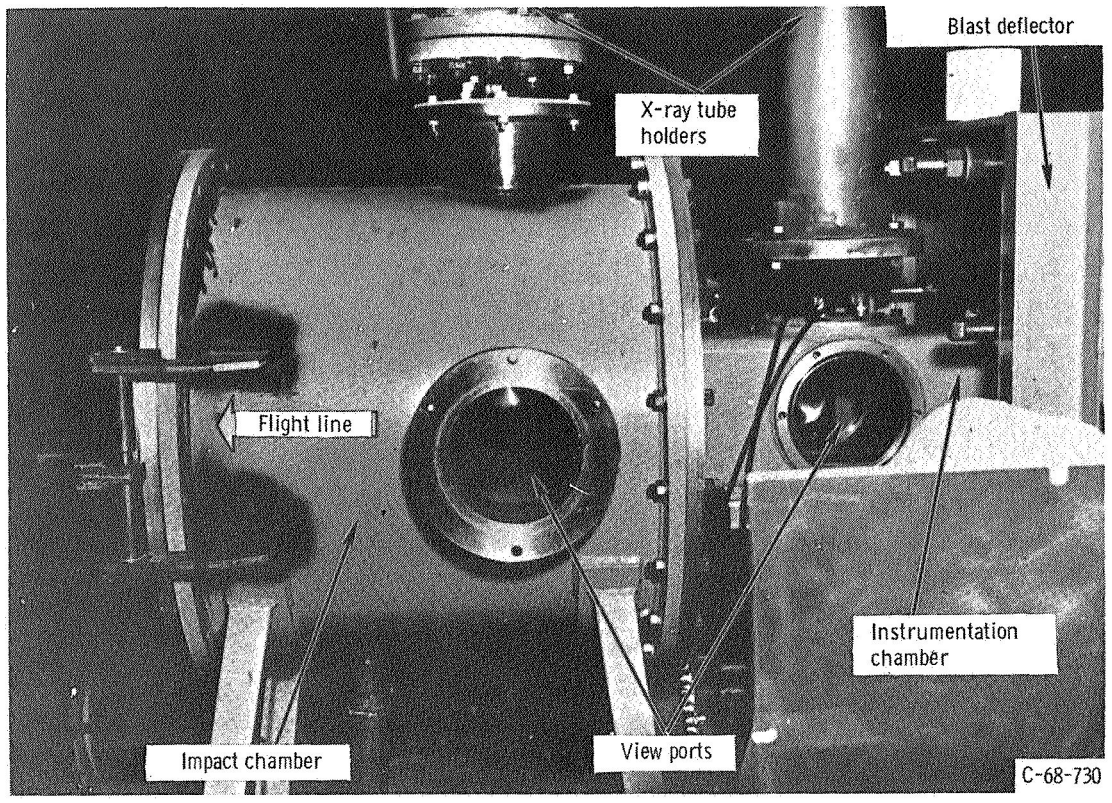

(b) Side view.

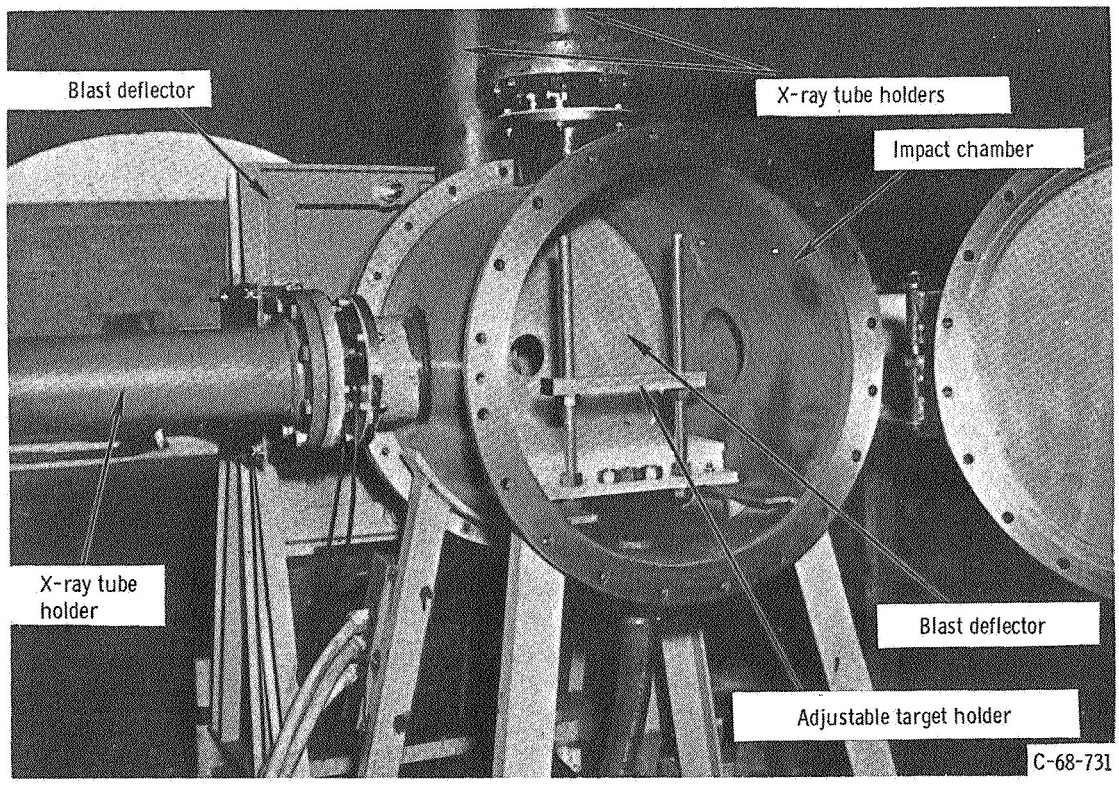

(c) Rear view.

Figure 1. - Concluded.

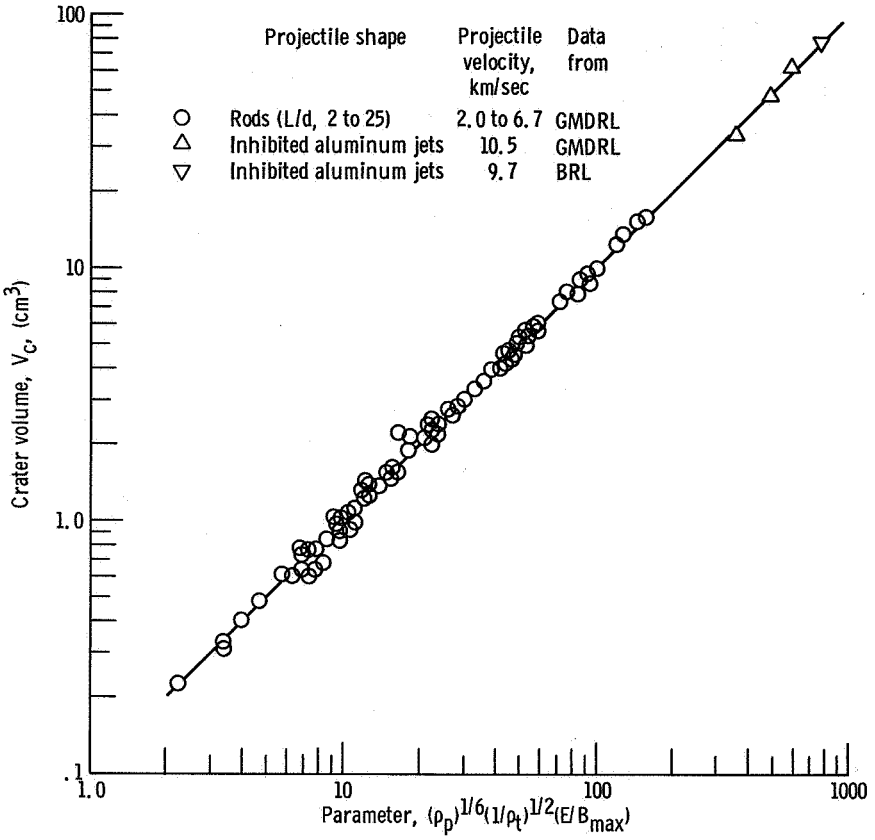

Figure 2. - Crater volume correlation (from ref. 2).

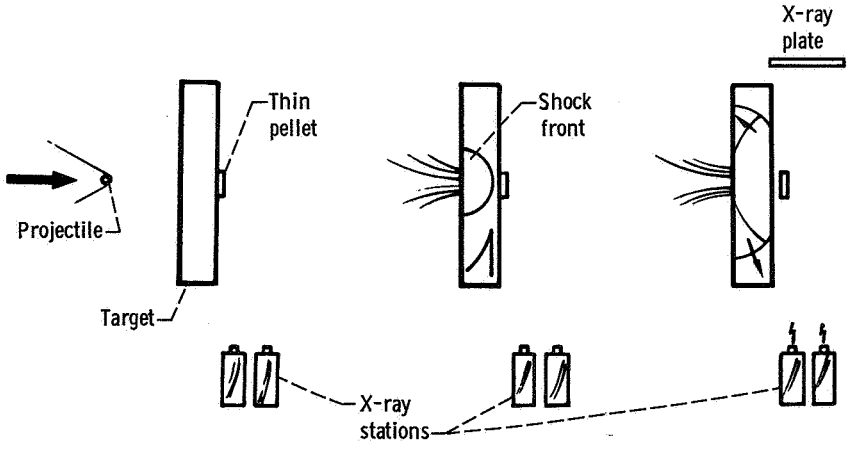

Figure 3. - Throwoff pellet technique.

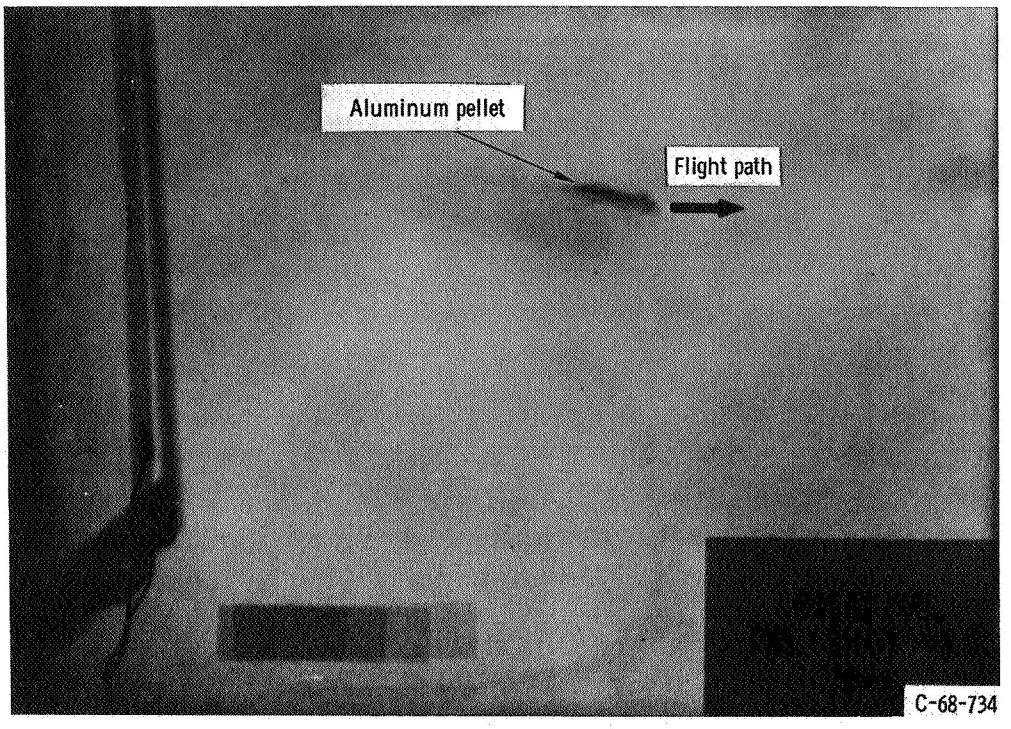

Figure 4. - X-ray of aluminum shaped-charge pellet at 11 kilometers per second. Projectile mass, 0.608 gram.

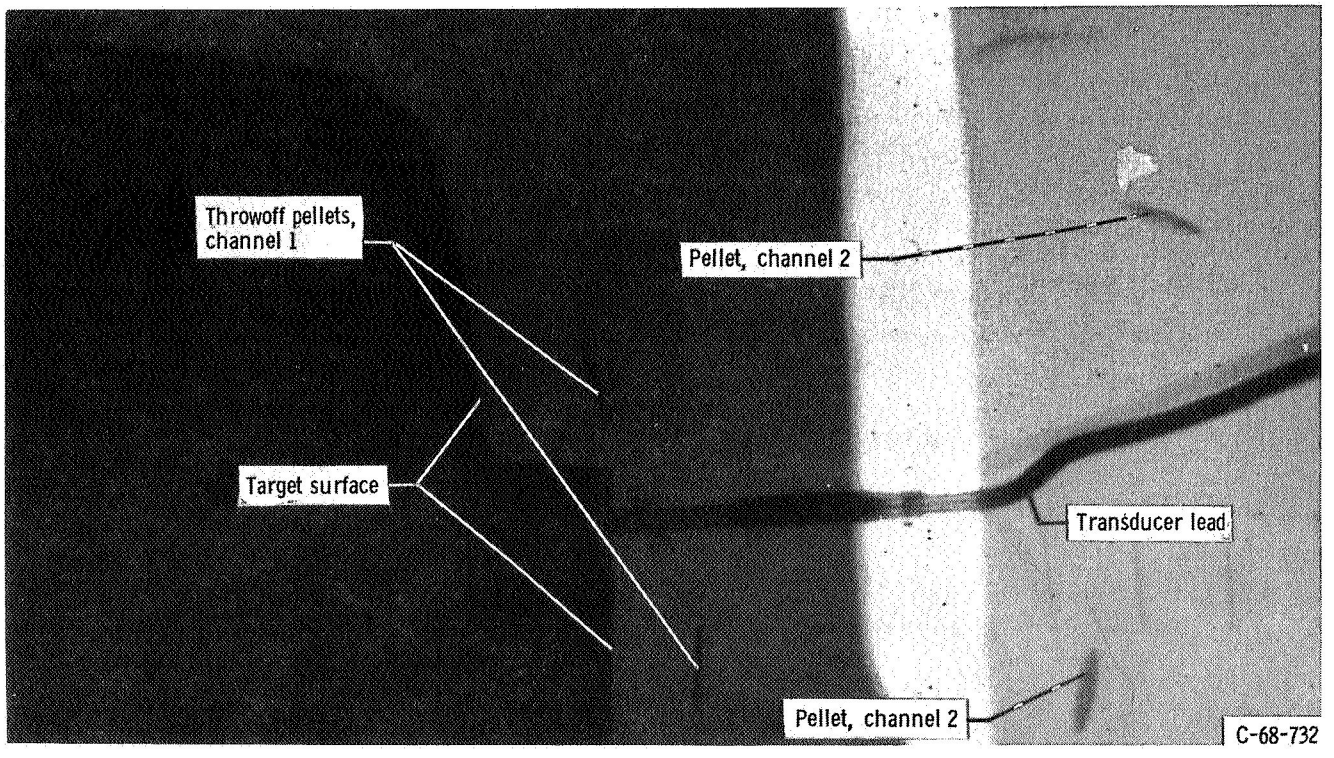

Figure 5. - X-ray of target response for shot 496.

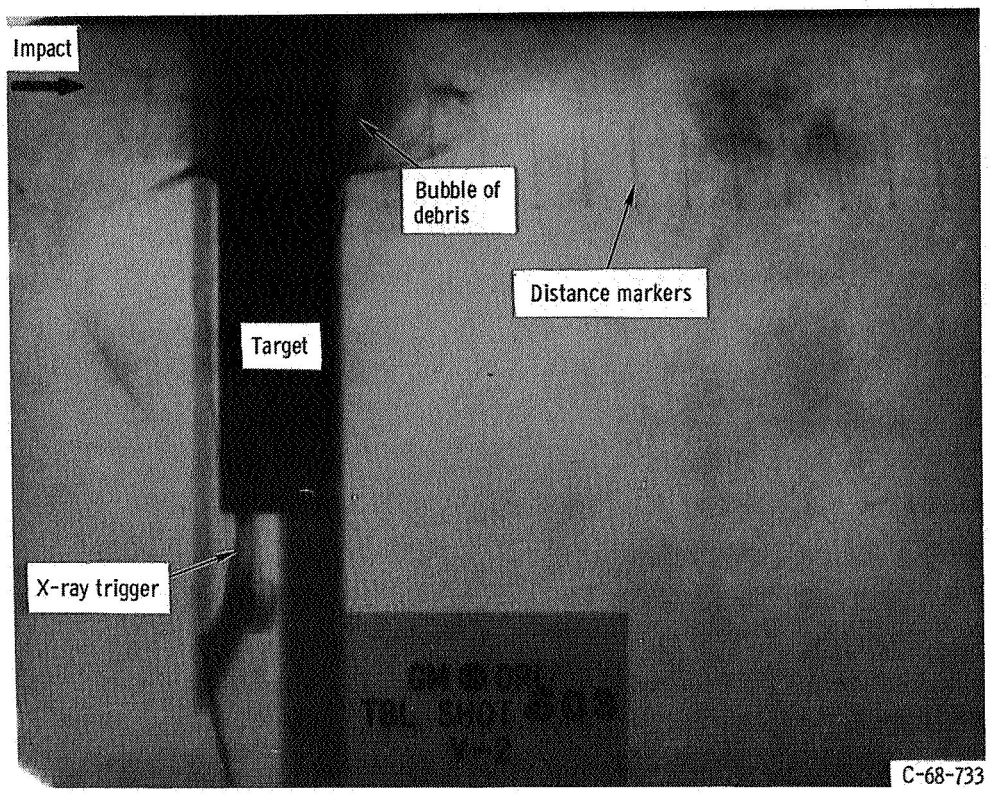

Figure 6. - X-ray of target response for shot 503.

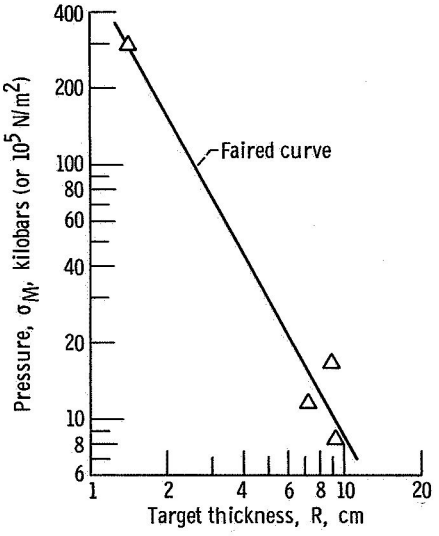

Figure 7. - Experimental results. Variation of maximum shock pressure with thickness (distance from impact) in 1100-0 aluminum.

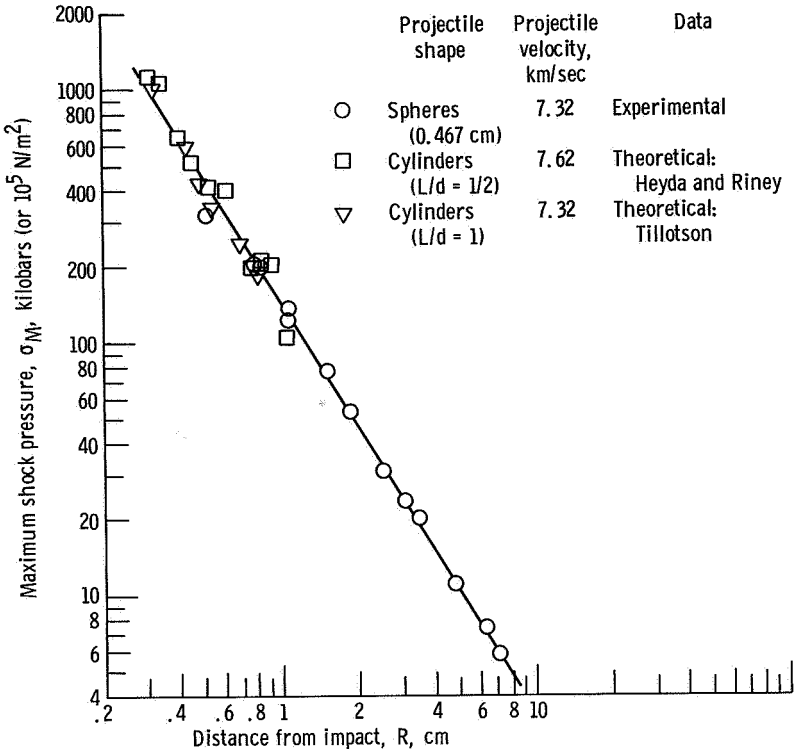

Figure 8. - Available data. Calculated and measured maximum shock-wave pressures generated by impacts of equivolume aluminum projectiles into 1100-0 aluminum targets (from ref. 3).

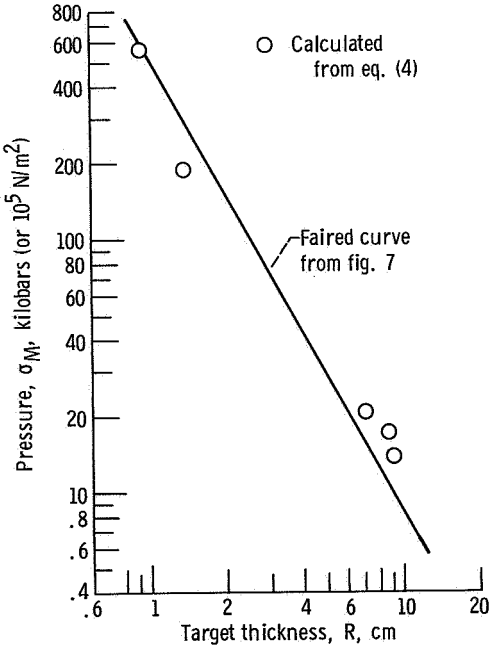

Figure 9. - Comparison of calculated and measured axial pressure variation in 1100-0 aluminum.

NATIONAL AERONAUTICS AND SPACE ADMINISTRATION
WASHINGTON, D.C. 20546
OFFICIAL BUSINESS

FIRST CLASS MAIL

POSTAGE AND FEES PAID
NATIONAL AERONAUTICS AND
SPACE ADMINISTRATION

POSTMASTER: If Undeliverable (Section 158
Postal Manual) Do Not Retur

"The aeronautical and space activities of the United States shall be conducted so as to contribute . . . to the expansion of human knowledge of phenomena in the atmosphere and space. The Administration shall provide for the widest practicable and appropriate dissemination of information concerning its activities and the results thereof."

— NATIONAL AERONAUTICS AND SPACE ACT OF 1958

NASA SCIENTIFIC AND TECHNICAL PUBLICATIONS

TECHNICAL REPORTS: Scientific and technical information considered important, complete, and a lasting contribution to existing knowledge.

TECHNICAL NOTES: Information less broad in scope but nevertheless of importance as a contribution to existing knowledge.

TECHNICAL MEMORANDUMS: Information receiving limited distribution because of preliminary data, security classification, or other reasons.

CONTRACTOR REPORTS: Scientific and technical information generated under a NASA contract or grant and considered an important contribution to existing knowledge.

TECHNICAL TRANSLATIONS: Information published in a foreign language considered to merit NASA distribution in English.

SPECIAL PUBLICATIONS: Information derived from or of value to NASA activities. Publications include conference proceedings, monographs, data compilations, handbooks, sourcebooks, and special bibliographies.

TECHNOLOGY UTILIZATION PUBLICATIONS: Information on technology used by NASA that may be of particular interest in commercial and other non-aerospace applications. Publications include Tech Briefs, Technology Utilization Reports and Notes, and Technology Surveys.

Details on the availability of these publications may be obtained from:

SCIENTIFIC AND TECHNICAL INFORMATION DIVISION

NATIONAL AERONAUTICS AND SPACE ADMINISTRATION

Washington, D.C. 20546